J Mol Med (2009) 87:31–41
DOI 10.1007/s00109-008-0402-7

ORIGINAL ARTICLE

Clinical variability in distal spinal muscular atrophy type 1 (DSMA1): determination of steady-state IGHMBP2 protein levels in five patients with infantile and juvenile disease

Ulf-Peter Guenther · Lusy Handoko · Raymonda Varon · Ulrich Stephani · Chang-Yong Tsao · Jerry R. Mendell · Susanne Lützkendorf · Christoph Hübner · Katja von Au · Sibylle Jablonka · Gunnar Dittmar · Udo Heinemann · Anja Schuetz · Markus Schuelke

Received: 2 March 2007 / Revised: 19 August 2008 / Accepted: 25 August 2008 / Published online: 18 September 2008

Abstract Distal spinal muscular atrophy type 1 (DSMA1) is caused by mutations in the immunoglobulin μ-binding protein 2 (*IGHMBP2*) gene. Patients with DSMA1 present between 6 weeks and 6 months of age with progressive muscle weakness and respiratory failure due to diaphragmatic palsy. Contrary to this "classic" infantile disease, we have previously described a DSMA1 patient with juvenile disease onset. In this paper, we present (1) a second juvenile case and (2) the first study of DSMA1 on protein level in patients with infantile (n=3) as well as juvenile (n=2) disease onset observing elevated residual steady-state IGHMBP2 protein levels in the patients with late onset DSMA1 as compared to those with classic DSMA1. Mutation screening in *IGHMBP2* revealed two patients compound heterozygous for a novel missense mutation (c.1478C→T; p.T493I) and

Electronic supplementary material The online version of this article (doi:10.1007/s00109-008-0402-7) contains supplementary material, which is available to authorized users.

U.-P. Guenther · S. Lützkendorf · C. Hübner · K. von Au · M. Schuelke (✉)
Department of Neuropediatrics,
Charité University Medical School of Berlin,
Augustenburger Platz 1,
13353 Berlin, Germany
e-mail: markus.schuelke@charite.de

U.-P. Guenther
Department of Biology, Chemistry and Pharmacy,
Free University Berlin,
Berlin, Germany

M. Schuelke
NeuroCure Clinical Research Center,
Charité University Medical School,
Berlin, Germany

L. Handoko
Institute of Biochemistry, University of Wuerzburg,
Wuerzburg, Germany

R. Varon
Institute of Human Genetics, Charité University Medical School,
Berlin, Germany

U. Stephani
Department of Neuropediatrics, University Hospital Kiel,
Kiel, Germany

C.-Y. Tsao · J. R. Mendell
Nationwide Children's Hospital,
Ohio State University,
Columbus, OH, USA

S. Jablonka
Institute for Clinical Neurobiology, University of Wuerzburg,
Wuerzburg, Germany

G. Dittmar
Mass Spectrometry Core Unit,
Max-Delbrück Center for Molecular Medicine,
Robert-Rössle-Str. 10 13125 Berlin, Germany

U. Heinemann · A. Schuetz (✉)
Protein Sample Production Facility,
Max-Delbrück Center for Molecular Medicine,
Robert-Rössle-Str. 10 13125 Berlin, Germany
e-mail: anja.schuetz@mdc-berlin.de

another previously described mutation. In lymphoblastoid cells of both patients, steady-state IGHMBP2 protein levels were reduced. In comparison to wild-type IGHMBP2, the p.T493I variant protein had an increased tendency to aggregate and spontaneously degrade in vitro. We verified a change in the physicochemical properties of the p.T493I variant which may explain the pathogenicity of this mutation. Our data further suggest that the age of onset of DSMA1 is variable, and we discuss the effect of residual IGHMBP2 protein levels on the clinical course and the severity of the disease.

Keywords IGHMBP2 · DSMA1 · Juvenile SMARD1 · Mutation · Steady-state protein levels · Protein aggregation · Genotype–phenotype relation

Introduction

Distal spinal muscular atrophy type 1 (DSMA1) often referred to as spinal muscular atrophy with respiratory distress type 1 (SMARD1) is characterized by dysfunction and progressive loss of α-motoneurons leading to neurogenic atrophy and weakness of trunk and limb muscles. In contrast to spinal muscular atrophy type 1 (SMA1), DSMA1 patients present with respiratory distress due to diaphragmatic paralysis between the first 6 weeks and 6 months of life [1, 2], and initial distal muscle weakness becomes generalized in the course of the disease. DSMA1 is an autosomal recessive disease and caused by mutations in the immunoglobulin μ-binding protein 2 (*IGHMBP2*) gene on chromosome 11q13.2-q13.4 [3]. IGHMBP2 is a member of the superfamily 1 of proteins from the helicase family [4], and unwinding activity has been demonstrated for IGHMBP2 in vitro on DNA substrates [5, 6]. Most DSMA1-causing missense mutations reside in the helicase domain which contains two recA-like subdomains and at least seven conserved motifs of amino acids (helicase motifs, Electronic supplementary material, Fig. 2) [7, 8]. In addition to its helicase domain, IGHMBP2 comprises two other structural elements near its C-terminus, an R3H single-stranded nucleic acid binding motif and a zinc-finger domain. In the cell, IGHMBP2 has been reported to be involved in the regulation of transcription and co-localizes with the RNA processing machinery [6, 9–11], but the precise cellular function of IGHMBP2 and the pathomechanism leading to DSMA1 still remain unknown. Although ubiquitously expressed, its enzymatic activity seems to be essential for the integrity of mainly α-motoneurons and cardiomyocytes [12].

Clinical and genetic heterogeneity of distal spinal muscular atrophies has been described [13, 14]. Recently, we reported a DSMA1 patient with late onset of respiratory distress and muscle weakness at 4.3 years [15]. This patient was a compound heterozygote for a large in-frame deletion and a missense mutation in *IGHMBP2*. Due to the unpredictable functional relevance of this genomic rearrangement, we did not know whether this case was just the exception to the rule or whether it widened the clinical spectrum of DSMA1. So far, no clear genotype–phenotype relation has been established for DSMA1.

In this paper, we report on the second case of DSMA1 with juvenile onset of respiratory distress and a novel missense mutation. We provide evidence that changes of physicochemical properties of the p.T493I IGHMBP2 variant might have an influence on steady-state IGHMBP2 levels in vivo. Additionally, we show that the abundance of residual IGHMBP2 protein correlates with the mode of clinical progression (infantile versus juvenile) in five DSMA1 patients.

Materials and methods

Patient no. 1 The girl is the first child of healthy non-consanguineous Caucasian parents. A younger brother is healthy. The pregnancy was complicated by premature labor at 7 months of gestation. Placental abruption necessitated a Caesarean section at 38 weeks of gestation, and her birth weight was 2,700 g. A bilateral varus foot deformity was treated by physiotherapy. She was able to walk unsupported at 12 months, but soon thereafter, she frequently stumbled and had problems to rise from the supine position. At three and a half years, she had developed distal muscular atrophy of the arms and legs, mild contractures of the wrist and elbow, a bilateral equinovarus foot deformity as well as generalized muscular hypotonia. Deep tendon reflexes were diminished in the arms and absent in the legs. Motor nerve conduction velocity was reduced in the median and peroneal nerves, while electromyography of the tibialis anterior muscle did not reveal any signs of denervation. Tongue fasciculations were absent. Histological examination of the quadriceps muscle revealed signs of neurogenic muscle atrophy. She was still able to walk at three and a half years but became wheelchair-dependent by the age of 4 years. Muscle weakness progressed and she required several orthopedic operations such as tendotomies at 6 years. After stabilization of the vertebral spine at 12 years, she suffered from painful swellings of the lower legs. From 9 years onwards, she required catheterization of the urinary bladder and was often constipated. She lost the ability to sit without support at 10 years. The pulmonary function was monitored over the years. The vital capacity declined continuously: 110% (5.3 years), 71% (7.2 years), and 58% (9.3 years). At 11 years, she had a severe restrictive ventilation disorder

with eventration of the right hemi-diaphragm, a vital capacity of 47%, a forced expiratory volume after one second of 53%, and a maximum end-expiratory flow at 75% expiration of 44%. All percentages refer to the residual capacity as compared to the lowest margin of the normal range. Subsequently, her pulmonary situation stabilized, but breathing had to be supported by continuous positive airways pressure and by nocturnal artificial ventilation. Serial chest X-rays on Fig. 1 illustrate the progressive paralysis of the diaphragm. At 15 years, she experienced difficulties swallowing and suffered from intermittent sinus tachycardia.

Patient no. 2 The boy is the only child of non-consanguineous parents of Caucasian origin and was delivered at term after an uncomplicated pregnancy. The birth weight was 2,650 g. From the beginning, his cry was persistently weak. At 3 months of age, his breathing became labored and he had difficulties feeding and failed to thrive. Left diaphragmatic paralysis was verified on chest radiographs. At 4 months, he had to be artificially ventilated and it was impossible to wean him again from the respirator. The child now depends on continuous ventilator support through a tracheostoma and is fed via a gastric tube. Additionally, his distal leg and hand muscles became progressively weak. At 5 months, he was unable to move his feet and developed contractures of his index fingers. A month later, the weakness had spread to the proximal muscle groups and he was unable to lift his legs and arms against gravity or grasp with his hands. This marked the nadir of his illness, after which he showed some improvement. At 9 months, he could lift his arms against gravity again but was still not able to bear weight on his legs. At 23 months, he was able to roll over. The findings of a standard muscle charting (five grades) were: neck flexors 3, shoulder abductors 4, elbow flexors 4, elbow extensors 4, wrist extensors 3, wrist flexors 3, finger flexors 1, knee extensors 3, hip flexors 2, ankle dorsiflexors 1, and trace movements in the toes. Generalized hypotonia and areflexia were present. Electromyography and nerve conduction studies proved widespread denervation with scattered large motor unit potentials and normal nerve conduction velocities without evidence of demyelination.

Additional patients For comparison, protein extracts of two previously described infantile (Px20 [1] and Px2 [15]) and one juvenile DSMA1 patient (Px1 [15]) were used in Western blot analysis. Additionally, protein extracts of the parents of patient no. 2 (F #2_II:1, F #2_II:2) and the mother of patient no. 1 (F #1_II:2) were loaded onto the gel. All *IGHMBP2* genotypes are provided at the lower panel of Fig. 3.

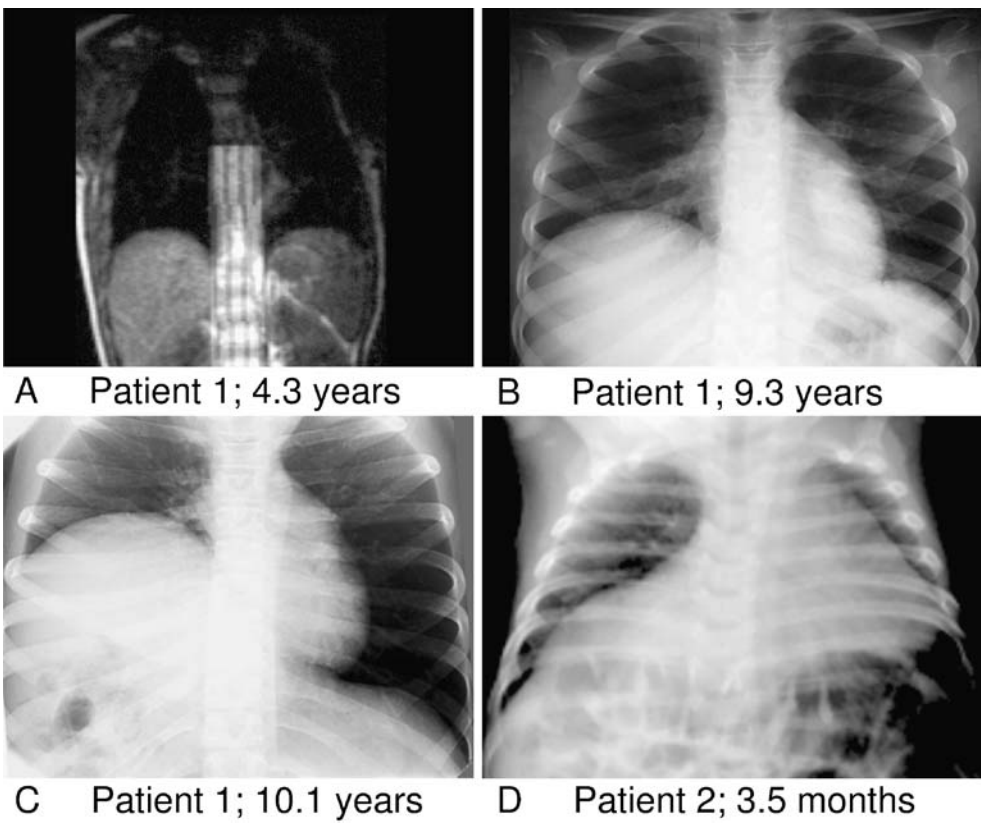

Fig. 1 Chest X-rays investigations (**a**–**c**) of patient no. 1 at ages 4.3, 9.3, and 10.1 years and (**d**) of patient no. 2 at 3.5 months. The series of patient no. 1 demonstrates the late onset of diaphragmatic paralysis *after* the onset of generalized muscle weakness

Genetic analysis After obtaining written informed consent of the patients' parents, heparinized blood or DNA samples of the patients were sent to our laboratory. Prior to this investigation, an *SMN1* deletion had been excluded in patient no. 1.

Epstein–Barr virus (EBV)-immortalized permanent lymphoblastoid cell lines (LCL) were established from heparinized blood of patients no. 1 and no. 2 [16]. Genomic DNA was prepared from peripheral blood samples or LCLs by standard salt extraction. For mutation screening, the coding exon and flanking intronic sequences of *IGHMBP2* were amplified by a standard polymerase chain reaction (PCR) protocol using a published primer set [3]. Additionally, we investigated the proximal promoter region (~1,000 bp) of the *IGHMBP2* gene through PCR amplification in three fragments by a standard PCR protocol (primers and conditions are available upon request). The ABI Prism BigDye® sequencing kit (Applied Biosystems, Weiterstadt, Germany) was used for bidirectional sequence analysis of purified PCR products. Analysis of mutation containing exons was repeated to ensure reproducibility. For segregation analyses, the relatives of the patient were also investigated for the mutations of the index patient. Mutations were numbered according to the current nomenclature [17] and referring accession numbers are the following: OMIM, (http://www.ncbi.nlm.nih.gov/Omim/) for IGHMBP2 [*600502], SMA1 [#253300] and DSMA1 [#604320]; GenBank (http://www.ncbi.nlm.nih.gov/Genbank/): *IGHMBP2* (NM_002180.1, NP_002171.1), *HPRT* (NM_000194.1), and *UBC* (NM_021009.3). A multiple alignment of orthologous *IGHMBP2* sequences was performed with the ClustalW software (http://www.ebi.ac.uk/clustalw).

Reverse transcription PCR (RT-PCR) on total RNA from LCLs was performed as described [15]. To exclude genomic rearrangements and to confirm the mutations on messenger RNA (mRNA) level, we performed Southern blotting with genomic DNA of patient no. 1 as described [15] and sequence analysis of the entire *IGHMBP2* coding sequence on complementary DNA (cDNA; primers and conditions are available upon request).

mRNA analysis IGHMBP2 mRNA transcript levels were determined in triplicate (*IGHMBP2/HPRT*) or duplicate (*IGHMBP2/UBC*) experiments in both patients and in three (*IGHMBP2/HPRT*) or two normal controls (*IGHMBP2/UBC*). We PCR-amplified a cDNA fragment between *IGHMBP2* exons 9 and 11 with the oligonucleotide primer set P33F (5′-GGC CTC AGA CAC CAT GTA CC-3') and P9R (5′-ACT TCG CCA GGG TTC CCT TTC-3′). Accumulation of PCR products was monitored through SYBR Green® incorporation on an ABI 7500 system (Applied Biosystems). Analysis of the dissociation curve at the end of the reaction assured the specificity of the PCR fragments and the absence of unspecific products. mRNA quantities were calculated with an efficiency calibrated 2Δ method [18] in relation to two housekeeping genes (*HPRT* and UBC [19]). The data were depicted as mean with standard deviation.

Western blot analysis Two affinity-purified rabbit polyclonal antisera were used to detect human IGHMBP2 protein. One antiserum, which we called the K14B antibody [10], was directed against a C-terminal peptide (α-peptide). The second antiserum (481 antibody) was directed against GST-tagged full-length mouse IGHMBP2 and was produced in rabbit according to the manufacturer's instructions (ImmunoGlobe, Himmelstadt, Germany).

Protein extracts were prepared from the LCLs of the patients as described previously [20] and separated on 7.5% sodium dodecyl sulfate (SDS) polyacrylamide gels. Proteins were electro-blotted to nitrocellulose membranes, blocked with 5% (*w*/*v*) milk powder in 1× TBS-T and probed with the K14B antibody for 90 min at room temperature followed by incubation with horseradish peroxidase-conjugated secondary antibody diluted 1:5,000 (Calbiochem, Nottingham, UK). Chemiluminescent detection was performed using the ECL reagents. The membrane was then washed thoroughly in conventional stripping buffer and re-probed with an immunogen affinity-purified polyclonal antiserum against human β-tubulin (Abcam, Cambridge, UK) as loading control. Before detection of IGHMBP2 on the same membranes with the second 481 antiserum, we verified the absence of the specific chemiluminescent signal originating from the former incubation. Western blot signals from at least three independent membranes blotted with the same protein extracts were then scanned and quantified densitometrically with the ImageJ software (http://rsb.info.nih.gov/ij/download.html). IGHMBP2 protein levels were depicted as the ratios between the integrated density of the IGHMBP2 bands and the loading control (β-tubulin). The data from at least three measurements were depicted as mean with standard deviation (Fig. 3). The significance of group differences was calculated with the non-parametric Mann–Whitney *U* test.

Genotyping of the nmd mice and Western blot of protein extracts from wild-type, heterozygous, and homozygous mutant mice Heterozygous *nmd* mice on a C57BL6 genetic background, which is the animal model of DSMA1 [21], were mated at a standard light–dark cycle of 12 h. Tail biopsy specimens were taken from each pup of the litter between P3 and P5. DNA was prepared after Proteinase K digestion and subsequent phenol–chloroform extraction. The first round of PCR was performed with the primers

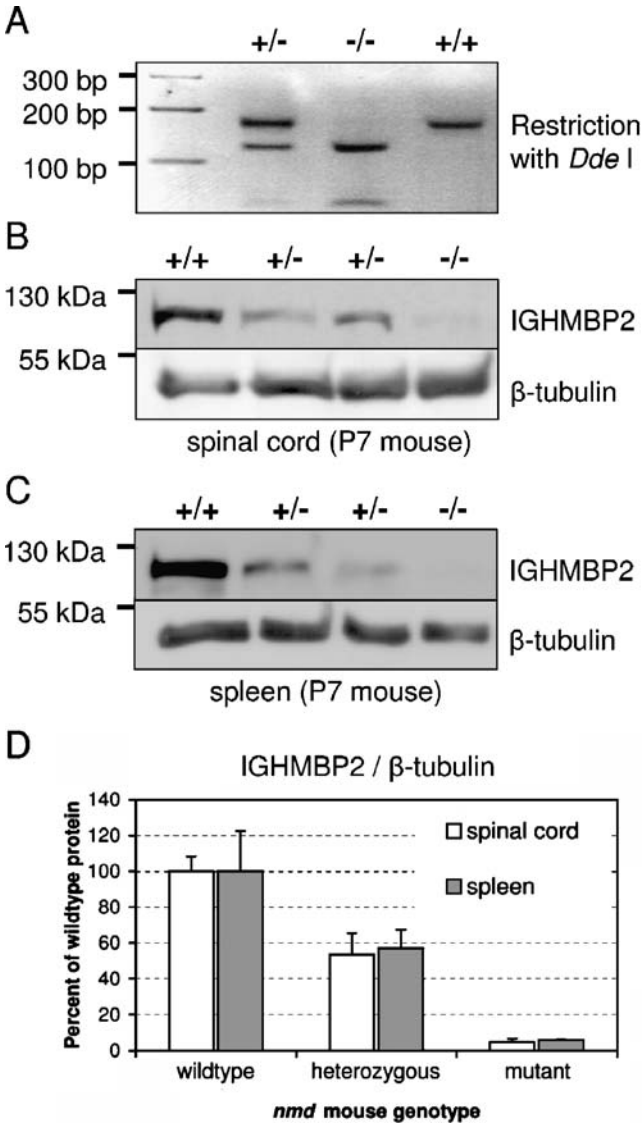

Fig. 2 Investigation of residual IGHMBP2 protein levels in *nmd* mice, the animal model of DSMA1, at postnatal day 7. **a** Genotyping of the *nmd* mice through restriction enzyme analysis with gain of a *Dde*I site in the presence of the intron 4 mutation. (+) wild-type and (−) mutant allele. **b** Determination of IGHMBP2 and β-tubulin protein levels in the spinal cord and in the spleen (**c**) of P7 animals by Western blot. Immunodetection of IGHMBP2 was performed with both K14B and 481 antibodies (only 481 is shown). **d** Comparison of the IGHMBP2/β-tubulin levels in spinal cord and in spleen did not reveal any significant difference for each combination of alleles. The mean of the protein levels from wild-type mice was set to 100%. All experiments were performed in triplicate, and the *whiskers* depict the standard deviation

S1874 (5-GCT GGA AAC GAT CAC ATA CCG-3) and S1875 (5-AGC TCC TGA TGA TCC AAT GG-3) and the second nested round with the primers S1876 (5-TCA CAG AGC ACT GAT GAC AC-3) and S1877 (5-TCT CTC TCT CAC ACA CAC ACA-3) which yielded a 169-bp product that was cleaved in the presence of the *nmd* mutation (IVS4+ 23A→G) into fragments of 123+46 bp (Fig. 2a). At P7, the animals were killed by atlantoaxial dislocation and their spinal cord and spleen were immediately removed and cryopreserved in liquid nitrogen. Preparation of the protein extracts and Western blotting was performed as described above.

Recombinant expression of wild-type IGHMBP2 and p.T493I variant protein The full open reading frame of human *IGHMBP2* including start and stop codon was RT-PCR amplified from RNA extracts of EBV-immortalized lymphoblastoid cells with tailed primers containing a *Sal*I (5′) and *Not*I (3′) restriction site and the proofreading Phusion® DNA polymerase (Finnzymes, Espo, Finland). The PCR product was cloned into the *Sal*I/*Not*I sites of the multiple cloning site of pET-28a (Novagen, Darmstadt, Germany) which appends a 6× His-Tag to the N-terminus. The correct sequence of the clone (pET-28a-wt-*IGHMBP2*) was verified by automatic sequencing. The c.1478C→T mutation (p.T493I) was introduced into pET-28a-wt-*IGHMBP2* using oligonucleotide-induced site-directed mutagenesis and subsequent selection of mutants with *Dpn*I [22]. The derived pET-28a-T493I-*IGHMBP2* clone was also sequenced. Both plasmids were electroporated into *Escherichia coli* Rosetta II cells (Novagen). Recombinant protein was produced in 2.5 l culture bottles that were grown at continuous shaking (225 rpm) at 37°C for around 4 h until an OD_{600}=0.8 was reached. After adjustment for 1 h at room temperature, protein expression was induced with 1 mM isopropyl-beta-D-thiogalactopyranoside (IPTG) and the cells incubated overnight at 16°C. The cells were harvested by centrifugation at 7,000×*g*, suspended in lysis buffer [1 M NaCl, 20 mM 4-(2-hydroxyethyl)-1-piperazineethanesulfonic acid (HEPES) pH 7.0, 20% glycerol, 0.01% NP40, 5 mM β-mercaptoethanol, 5 mM $MgCl_2$, and the proteinase inhibitors: 0.7 μg/ml Pepstatin, 0.1 mM AEBSF, 2 μg/ml Apronitin, 0.5 μg/ml Leupeptin], and disrupted by sonification at 4°C (ultrasonic disintegrator UP100H, Hielscher, Teltow, Germany, 5×30 s at 100 W, 100% amplitude and intermittent cooling on ice for 30 s). The ultracentrifugation supernatant (centrifugation at 50,000×*g* for 30 min) with the biochemically active protein was loaded onto a 5-ml HiTrap® chelating column (GE Healthcare, Munich, Germany, charged with nickel) for affinity purification with the ÄKTA Purifier® system (GE Healthcare). The protein was eluted with a linear 25–500 mM imidazole gradient in 20 mM HEPES pH 7.0, 500 mM NaCl, 10% glycerol, 5 mM $MgCl_2$, 5 mM β-mercaptoethanol, and 0.1 mM AEBSF. The IGHMBP2 containing eluate was dialyzed against 20 mM HEPES pH 7.0, 500 mM NaCl, 5% glycerol, 5 mM $MgCl_2$, 5 mM β-mercaptoethanol, and 0.1 mM AEBSF and concentrated to 10 mg/ml with an ultracentrifugation concentrator (Vivaspin 4 ml, 50,000 MWCO, Sartorius, Goettingen, Germany). One milligram

protein was subsequently separated by size exclusion chromatography on a Superdex® 200 column (10× 300 mm, GE Healthcare) at a flow rate of 0.5 ml/min that had been calibrated with proteins of different sizes (HMW Kit, GE Healthcare) before. The fractions of the different elution peaks were pooled and concentrated (Fig. 4a). Each of the aforementioned steps was controlled by SDS–polyacrylamide gel electrophoresis (PAGE) and subsequent Coomassie or silver staining. The pooled fractions of the 11.5 ml peak produced a predominant band of the expected molecular size of ~115 kDa and two minor bands representing degraded IGHMBP2 fragments as verified by mass spectrometry (see below). The other peaks (e.g., at 15.8 ml) comprised low-molecular-weight degradation products.

Mass spectrometry Peptides were generated by in-gel digestion as described [23]. The peptide solution was separated by reverse phase chromatography on an Acquity UPLC (Waters, Milford, MA, USA) and analyzed by electrospray ionization mass spectrometry on a Q-TOF premier mass spectrometer (Waters). Peptide spectra were assigned using the MASCOT software (Matrix Science).

Thermal shift assay The environmentally sensitive fluorescent dye Sypro Orange® (Invitrogen, Carlsbad, CA, USA) was used to monitor protein unfolding with respect to temperature. The thermal shift assay was conducted in triplicate using the iQ5 Multicolor real-time PCR detection system (Bio-Rad, Munich, Germany). Twenty micrograms recombinant wt and p.T493I IGHMBP2 protein from the 11.5 ml tetramer peak (Fig. 4c) was dissolved in 30 µl 20 mM HEPES pH 7.0, 250 mM NaCl, 5% glycerol, 5 mM $MgCl_2$, and 5 mM β-mercaptoethanol and mixed with 20 µl 2.5× Sypro Orange® (in water) in a PCR tube. The sample was heated from 20°C to 100°C with a rate of 1°C per minute. Changes in fluorescence intensity were monitored, and the wavelengths for excitation and emission were 490 and 530 nm, respectively. Melting temperatures (T_m, the temperature midpoint for the protein unfolding transition) were determined from the peak value of the first derivative curve.

Limited trypsination One hundred micrograms of the dialyzed and concentrated recombinant wt and p.T493I IGHMBP2 protein from the 11.5 ml tetramer peak (Fig. 4c) was incubated in a total volume of 300 µl of 1× phosphate buffered saline to which trypsin had been added to a final concentration of 3 mg/l (low trypsin) or 30 mg/l (high trypsin) and incubated at 16°C. At the indicated time intervals (Fig. 5), 30 µl aliquts were removed, immediately boiled in 2× Laemmli loading buffer, and subsequently frozen at −20°C until SDS-PAGE analysis.

Results

A novel missense mutation (p.T493I) in two DSMA1 patients with different clinical courses

In this report, we investigated two patients with the clinical features of DSMA1 but different clinical courses in whom respiratory distress appeared at 3.5 months (patient no. 2) versus 10 years of age (patient no. 1). In the juvenile DSMA1 patient, we identified compound heterozygous mutations in *IGHMBP2* leading to non-conservative amino acid substitutions p.L361P (c.1082T→C, exon 8) and p.T493I (c.1478C→T, exon 10) confirming the diagnosis of DSMA1. Segregation analysis in the family revealed p.L361P to segregate in the paternal, while p.T493I segregated in the maternal line (Electronic supplementary material, Fig. 1). The c.1082T→C transition was identified previously in four patients with infantile onset of DSMA1 [1, 24].

The patient with infantile DSMA1 was compound heterozygous for the same nucleotide transition in exon 10 (c.1478C→T, p.T493I) and a nonsense mutation in exon 13 (c.2363C→T, p.R788X; Electronic supplementary material, Fig. 1) that had been described in two infantile DSMA1 patients before [1].

The here identified c.1478TC→T transition is novel, and we did not find this variant in over 300 Caucasian controls which excludes a polymorphism [25]. Sequence analysis of the entire coding sequence of *IGHMBP2* on cDNA level in both patients did not reveal any other alterations. Additionally, we analyzed the promoter region of the *IGHMBP2* gene (~1,000 bp upstream of the translation initiation codon) in both patients but did not find any deviations from the standard sequence. Southern blot analysis of the DNA from patient no. 1 excluded major deletions or rearrangements at the *IGHMBP2* locus (data not shown). Multiple alignment of vertebrate orthologs and a homologous yeast sequence [5] shows a strong evolutionary conservation of the p.T493 residue (Electronic supplementary material, Fig. 2). These data strongly suggest c.1478C→T (p.T493I) to be a pathogenic mutation, causing DSMA1 in combination with a second mutation on the other allele in both patients.

Steady-state IGHMBP2 protein levels are reduced in DSMA1 patients

Taking advantage of cell lines from both the above described and a further three patients with infantile and juvenile onset of disease, we investigated whether the abundance of residual IGHMBP2 protein might be related to the different manifestation age of the disease. As p.T493I is not located in proximity to any of the known helicase

motifs that are important for the enzymatic activity (Electronic supplementary material, Fig. 2), we speculated that this mutation might rather affect transcriptional mRNA levels or protein concentrations.

As immortalized LCLs were the only patient material available, we first investigated whether changes in this cell type do reflect those in the spinal cord, the primary site of pathogenesis. For that, we investigated IGHMBP2 protein levels in the *nmd* mouse, the animal model for DSMA1 [15, 21]. As mouse lymphocytes cannot be immortalized with the Epstein–Barr virus, we investigated IGHMBP2 protein levels in homogenates of spleen, which predominantly contains B lymphocytes, and spinal cord of wild-type, heterozygous, and homozygous *nmd* mice. All investigated mice were littermates from heterozygous *nmd* parents. The reduction of the IGHMBP2/β-tubulin protein ratio went exactly parallel in spinal cord and in spleen (and thus within B lymphocytes) without any significant differences between the two organs for all the allelic combinations of the *nmd* mouse (Fig. 2b–d). Thus, we conclude that the

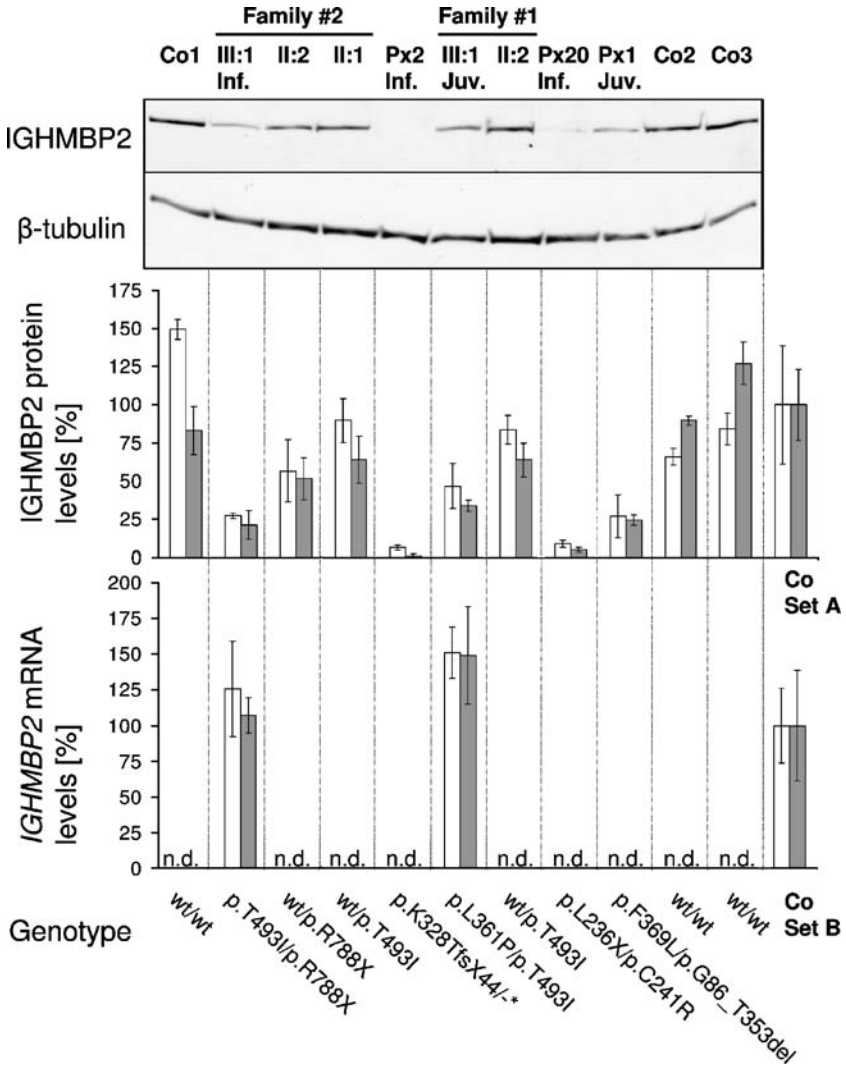

Fig. 3 Quantification of IGHMBP2 mRNA transcript and protein steady-state levels. *Upper panel*: Protein extracts from lymphoblastoid cells of three controls (Co1, Co2, Co3), patient no. 2 (*F #2_III:1*) and his parents (*F #2_II:1*, *F #2_II:2*), patient no. 1 (F #1_III:1) and her mother (*F #1_II:2*), two infantile (*Inf.*) DSMA1 patients (*Px2*, *Px20*), and a further juvenile (*Juv.*) DSMA1 patient (*Px1*) were loaded. Incubation with an anti β-tubulin antibody was used for loading control. Western blot analysis was performed using the affinity-purified antisera K14B and 481 (blot not shown). *Middle panel*: Densitometric quantification of the signals from three independent Western blots after incubation with two different antibodies, K14B (*white bars*) and 481 (*gray bars*). "Co set A" is the summation of all three controls depicted in the *upper panel*. *Lower panel*: *IGHMBP2* mRNA transcript levels were determined in two TaqMan assays and were expressed as the ratio of *IGHMBP2* to two housekeeping genes, *HPRT* (*white bars*) and *UBC* (*gray bars*). The genotypes of the patients are given *below the panel*. The *bars* depict the arithmetic mean of the measurements and the *whiskers* one standard deviation. "Co set B" comprises three controls in the case of the *HPRT* and two in the case of the *UBC* reference gene. These controls are not identical to "Co set A"

quantification of residual IGHMBP2 steady-state protein levels in the patient LCLs may reflect the situation in the α-motoneurons, the primary site of neurodegeneration.

Next, we examined IGHMBP2 protein levels from the patient LCLs, their parents, and other infantile and juvenile DSMA1 cases (Fig. 3, upper panel). The IGHMBP2 to β-tubulin ratio in patient no. 1 (F #1_III:1) was at 40±12% of healthy controls. In patient no. 2 (F #2_III:1), the ratio was reduced to 24±8%. In agreement with this finding, we observed that also other infantile DSMA1 patients had lower IGHMBP2 levels (12±10%; $n=3$) than juvenile DSMA1 patients (33±13%; $n=2$). These differences were significant ($p<0.005$) as determined by the Mann–Whitney U test.

p.T493I reduces steady-state IGHMBP2 protein levels in vivo

Interestingly, both parents (F #1_II:2 and F #2_II:1) who are heterozygous carriers of the p.T493I mutation have IGHMBP2 to β-tubulin ratios of approximately 75% of controls. In line with this, the mother of patient no. 2 who shares the nonsense mutation with her son but is wild-type on the other allele has approximately half the IGHMBP2 levels of controls (while her son has approximately 25%). Taken together, these findings suggest that the p.T493I mutation leads to reduced steady-state levels of IGHMBP2 protein by around 50% (Fig. 3, middle panel).

We wondered whether this reduction of IGHMBP2 protein was already caused on mRNA transcript level or on the level of the protein itself. We thus additionally determined the *IGHMBP2* mRNA transcript levels through RT-PCR. Normalization to two housekeeping genes revealed even slightly elevated *IGHMBP2* mRNA transcript levels in both patients. The relative *IGHMBP2* transcript

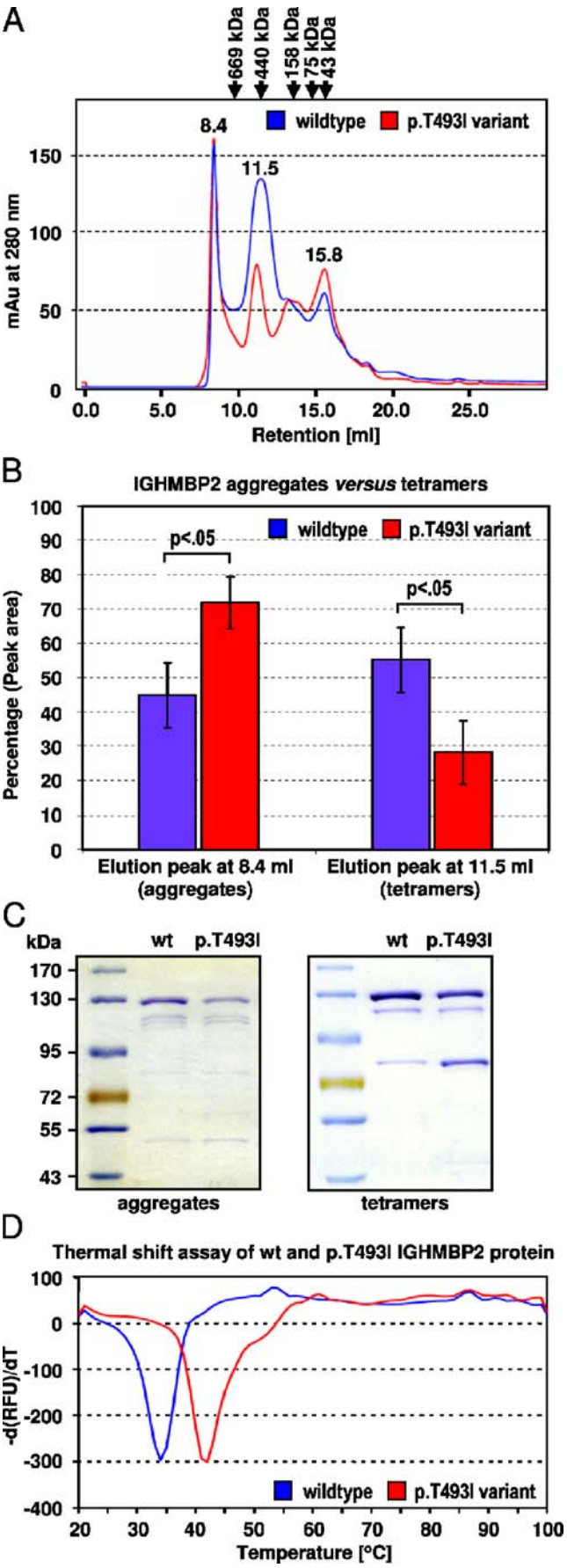

Fig. 4 Biochemical characterization of wild-type and variant IGHMBP2. **a** Elution diagrams after size exclusion chromatography of recombinant wild-type (*blue*) and p.T493I variant (*red*) IGHMBP2. The Superdex® 200 column (10×300 mm) had been calibrated with thyroglobulin (669 kDa), ferritin (440 kDa), aldolase (158 kDa), conalbumin (75 kDa), and ovalbumin (43 kDa). The peak at 8.4 ml corresponds to high-molecular-weight protein aggregates, the peak at ~11.5 ml to homotetramers (~440 kDa), and the peak at 15.8 ml to low-molecular-weight degradation products. **b** Quantitative analysis of the area below the 8.4- and 11.5-ml elution peaks. The sum of both peak areas was set to 100% and the *columns* depict the relative contribution of the aggregates and the homotetramers. The *whiskers* depict the standard deviation from three independent protein isolations and chromatographic runs. **c** Denaturating SDS-PAGE of the concentrated fractions of the aggregate and homotetrameric peaks. The homotetrameric protein was further investigated by thermal shift assay and limited tryptic proteolysis. **d** Thermal shift assay with homotetrameric wild-type and p.T493I variant IGHMBP2. The 9°C shift in the melting temperature points towards a higher thermal stability of the variant protein. The melting curves are depicted as the first derivative against the temperature. All experiments were performed in triplicates

numbers were increased in patient no. 1 to 157±23% and in patient no. 2 to 123±27% if compared to control subjects (Fig. 3, lower panel). These results only achieved marginal significance if referred to *HPRT* ($p=0.03$); however, they demonstrate the reduced steady-state IGHMBP2 levels in the presence of the c.1478C→T (p.T493I) mutation to be rather the cause of reduced translation or protein degradation than diminished mRNA levels.

p.T493I affects physicochemical properties of the helicase domain

To further analyze the effect of the p.T493I variant on the protein level, we purified recombinantly expressed full-length wild-type and variant IGHMBP2 protein. First, we determined the oligomerization state of wild-type and variant IGHMBP2 through size exclusion chromatography revealing the presence of predominantly homotetramers with a molecular weight of around 440 kDa. We additionally found a protein aggregate peak close to the exclusion volume of the column that was, in relation to the homotetramer, significantly ($p<0.05$) larger for the p.T493I variant (Fig. 4a,b). Both aggregate and homotetramer peaks of wild-type and variant IGHMBP2 resolved into a predominant band at ~115 kDa on SDS-PAGE, resembling the expected size of the full-length IGHMBP2 protein. The homotetrameric protein fractions additionally revealed a degradation band at ~75 kDa (Fig. 4c) that is more prominent in the p.T493I variant. As determined by mass spectrometry (data not shown), this fragment comprises the N-terminal amino acid residues 1–674, bearing the entire helicase domain (aa 18–644), but excluding the C-terminal R3H and zinc finger domain.

Further, we examined the impact of the p.T493I variant on protein stability by protein unfolding through thermal denaturation. For both wild-type IGHMBP2 and p.T493I variant, we observed a single melting transition, revealing a cooperative unfolding (melting as a single unit). The shift of the melting temperature from 34°C in wild-type to 43°C in the p.T493I variant (Fig. 4d) indicates a higher thermal stability for the variant protein.

Next, we assessed the susceptibility of IGHMBP2 proteins to proteolytic degradation and we performed a limited trypsination with both wild-type and IGHMBP2 variant. As a result, the tryptic degradation products are similar to the spontaneous degradation band that is primarily present in the p.T493I variant (Fig. 5). Interestingly, the 75-kDa degradation product of the p.T493I variant protein is much more resistant against tryptic proteolysis than its wild-type counterpart (Fig. 5, lower panel).

Taken together, the data indicate a change of in vitro physicochemical properties of the helicase domain in the p. T493I variant.

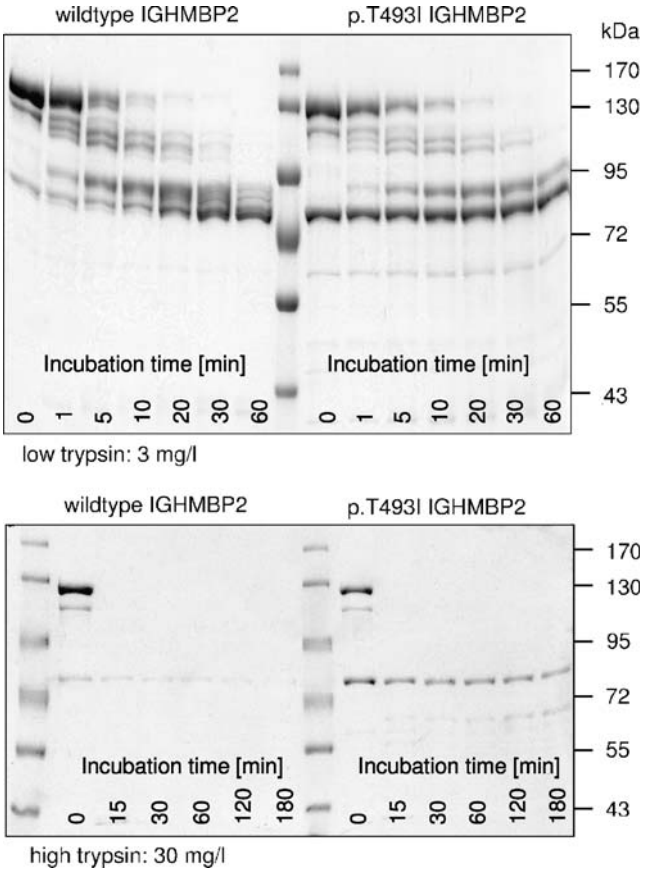

Fig. 5 Limited trypsination of wild-type and variant IGHMBP2 using different trypsin concentrations (3 and 30 mg/l). Both wild-type and variant IGHMBP2 result in the same 75 kDa degradation product. However, the 75 kDa band containing the helicase domain bearing the p.T493I mutation is more resistant against tryptic digestion as its wild-type counterpart even at high trypsin concentrations (*lower panel*). Spontaneous and tryptic degradation products appear to be identical as verified by mass spectrometry (data not shown)

Discussion

The course of DSMA1 is variable. Although most patients suffer from the infantile type of DSMA1 and present with respiratory failure between 6 weeks to 6 months of life [1, 2], we have recently reported on a patient with onset of respiratory distress at the age of 4.3 years, which we designated the "juvenile" type DSMA1 [15]. Here, we report on a second case of juvenile DSMA1 and attempt to correlate clinical observations with biochemical and molecular genetic data. We investigated two DSMA1 patients who were compound heterozygous for the c.1478C→T (p.T493I) missense mutation in conjunction with a second but already published mutation on the other allele (Electronic supplementary material, Fig. 1). Intriguingly, patient no. 1 first developed dyspnea at the age of 10 years, whereas patient no. 2 already became ventilator-dependent by the age of 4 months. The disease progression in patient no. 2 was within the time frame of other infantile DSMA1

patients, but the onset of DSMA1 was exceptionally late in patient no. 1, similar to a single patient with a rearrangement at the *IGHMBP2* locus whom we had reported earlier (Px1 [15]).

Quantification of residual IGHMBP2 protein levels revealed significant differences between patients no. 1 and no. 2. These differences remained significant (p=0.0032 for the 418 antibody and p=0.0067 for the K14B antibody) when patient no. 2 was grouped with two other infantile DSMA1 patients (Px20; [1] and Px2; [15]) and patient #1 with the other juvenile DSMA1 patient (Px1 [15], $p<$ 0.005). However, the residual protein levels did not differ significantly (p=0.275 for the 418 antibody and p=0.827 for the K14B antibody) if we compared patient no. 2 (infantile onset) only with Px1 (juvenile onset [15]).

Despite the reduction of IGHMBP2 protein levels, *IGHMBP2* mRNA levels were not decreased in both patients. This suggests that the c.1478C→T (p.T493I) missense mutation rather affects specific protein abundance. Determination of IGHMBP2 protein levels in heterozygous carriers of p.T493I consistently showed a reduction of 25% if compared to controls which implies a ~50% decrease in steady-state levels of the p.I493 IGHMBP2 variant in vivo.

Further analysis of recombinant wild-type and variant IGHMBP2 protein hinted towards the pathogenetic principle of the p.T493I mutation through an increased tendency to form high-molecular-weight aggregates and to spontaneously degrade.

Although there has been a growing appreciation that protein function, stability, and aggregation are intrinsically linked, it is not yet clearly established how the change in these physicochemical properties of a protein impact on its steady-state levels in vivo [26]. It is known that misfolded or abnormally folded proteins are selectively targeted for degradation [26, 27]. Our results suggest that the conformational and structural alterations brought about by the p.T493I variant may be recognized by the cellular degradation machinery, possibly via its higher aggregation levels, and could thus account for the reduced cellular abundance of the p.T493I variant.

Although we found higher residual steady-state IGHMBP2 levels in patients with juvenile DSMA1, we are cautious whether this might correlate with the onset of disease. Infantile DSMA1 patient no. 2 has one allele with a nonsense mutation, while the juvenile DSMA1 patient no. 1 is a compound heterozygote for two missense mutations. Thus, differences in residual IGHMBP2 levels may simply reflect whether both or only one allele contribute to the steady-state level. We have recently published an infantile DSMA1 case who was compound heterozygous for a p.H445P missense mutation and a c.1235+3A→G splice site mutation [2]. This splice site mutation still allowed for ~24% wild-type transcripts to be produced that were, however, not enough to avert the disease phenotype in the patient. We thus can only speculate that the threshold for functional IGHMBP2 protein must be somewhere between 25% and 50% to modify the disease.

It is noteworthy that Cox et al. [21] found evidence for a modifying (genetic) factor that influenced onset and progression of the disease in a mouse model of DSMA1, the *nmd* mouse. Thus, we cannot rule out that the slow clinical progression seen in the juvenile DSMA1 patients might be due to the presence of a similar "neuron-protective" allele in humans.

It should further be noted that the experiments in this study were conducted with extracts from LCLs which are not the primarily affected cell type in DSMA1 even if we have provided evidence in the mouse that IGHMBP2 expression levels are similar in spinal chord tissue and spleen homogenates whose major constituents (50–60%) are $CD19^+$ B lymphocytes [28]. Those $CD19^+$ cells resemble LCLs in many respects [16, 29]. Together with strong circumstantial evidence from the literature [30], we think that LCLs are a reasonably good "model system" to investigate pathogenesis of DSMA1 on biochemical level.

We are aware that this investigation with two juvenile DSMA1 patients can only be a pilot study and more experimental evidence has to be collected to prove a relationship between functional residual IGHMBP2 protein levels and the disease course. Moreover, it will be necessary to assess the effect of different mutations on the catalytic activity of IGHMBP2 in vitro, especially for those mutations which have been found in patients with juvenile onset of the disease.

In conclusion, we present the second case with juvenile onset of DSMA1 thus underlining the variable course of the disease. Additionally, we provide evidence that the physicochemical alterations of the IGHMBP2 protein brought about by a novel missense mutation lead to decreased steady-state IGHMBP2 levels in vivo. Furthermore, our finding of higher steady-state IGHMBP2 levels in juvenile DSMA1 patients suggest that even variant protein with residual enzymatic activity might exert a certain protective effect if present in sufficient quantity.

Acknowledgments We thank the patients and their families for participation in this study. G. Koch, Children's Hospital Hagen, and A. Hahn, Department of Neuropediatrics, Kiel University, contributed to the medical management of one patient. We thank Véronique Dutrannoy for providing *HPRT* primers and help in the RT-PCR TaqMan assay and Dr. Dietrich Carlhoff from GE Healthcare for his continuous help and counseling regarding the ÄKTA FPLC system. The work was supported by grants of the Deutsche Forschungsgemeinschaft (HU 408/3-2 and HU 408/3-3), the Charité (Rahel-

Hirsch-Fellowship to K.v.A.), and by a generous donation of the parents' self help group "Helft dem muskelkranken Kind, Hamburg e.V.". The Protein Sample Production Facility at the Max Delbrück Center is funded by the Helmholtz Association of German Research Centers.

References

1. Grohmann K, Varon R, Stolz P, Schuelke M, Janetzki C, Bertini E, Bushby K, Muntoni F, Ouvrier R, Van ML, Goemans NM, Lochmuller H, Eichholz S, Adams C, Bosch F, Grattan-Smith P, Navarro C, Neitzel H, Polster T, Topaloglu H, Steglich C, Guenther UP, Zerres K, Rudnik-Schoneborn S, Hubner C (2003) Infantile spinal muscular atrophy with respiratory distress type 1 (SMARD1). Ann Neurol 54:719–724
2. Guenther UP, Varon R, Schlicke M, Dutrannoy V, Volk A, Hubner C, von Au K, Schuelke M (2007) Clinical and mutational profile in spinal muscular atrophy with respiratory distress (SMARD): defining novel phenotypes through hierarchical cluster analysis. Hum Mutat 28:808–815
3. Grohmann K, Schuelke M, Diers A, Hoffmann K, Lucke B, Adams C, Bertini E, Leonhardt-Horti H, Muntoni F, Ouvrier R, Pfeufer A, Rossi R, Van ML, Wilmshurst JM, Wienker TF, Sendtner M, Rudnik-Schoneborn S, Zerres K, Hubner C (2001) Mutations in the gene encoding immunoglobulin mu-binding protein 2 cause spinal muscular atrophy with respiratory distress type 1. Nat Genet 29:75–77
4. Koonin EV (1992) A new group of putative RNA helicases. Trends Biochem Sci 17:495–497
5. Biswas EE, Nagele RG, Biswas S (2001) A novel human hexameric DNA helicase: expression, purification and characterization. Nucleic Acids Res 29:1733–1740
6. Molnar GM, Crozat A, Kraeft SK, Dou QP, Chen LB, Pardee AB (1997) Association of the mammalian helicase MAH with the pre-mRNA splicing complex. Proc Natl Acad Sci U S A 94:7831–7836
7. Cheng Z, Muhlrad D, Lim MK, Parker R, Song H (2007) Structural and functional insights into the human Upf1 helicase core. EMBO J 26:253–264
8. Tanner NK, Linder P (2001) DExD/H box RNA helicases: from generic motors to specific dissociation functions. Mol Cell 8:251–262
9. Fukita Y, Mizuta TR, Shirozu M, Ozawa K, Shimizu A, Honjo T (1993) The human S mu bp-2, a DNA-binding protein specific to the single-stranded guanine-rich sequence related to the immunoglobulin mu chain switch region. J Biol Chem 268:17463–17470
10. Grohmann K, Rossoll W, Kobsar I, Holtmann B, Jablonka S, Wessig C, Stoltenburg-Didinger G, Fischer U, Hubner C, Martini R, Sendtner M (2004) Characterization of Ighmbp2 in motor neurons and implications for the pathomechanism in a mouse model of human spinal muscular atrophy with respiratory distress type 1 (SMARD1). Hum Mol Genet 13:2031–2042
11. Shieh SY, Stellrecht CM, Tsai MJ (1995) Molecular characterization of the rat insulin enhancer-binding complex 3b2. Cloning of a binding factor with putative helicase motifs. J Biol Chem 270:21503–21508
12. Maddatu TP, Garvey SM, Schroeder DG, Hampton TG, Cox GA (2004) Transgenic rescue of neurogenic atrophy in the nmd mouse reveals a role for Ighmbp2 in dilated cardiomyopathy. Hum Mol Genet 13:1105–1115
13. Maystadt I, Zarhrate M, Landrieu P, Boespflug-Tanguy O, Sukno S, Collignon P, Melki J, Verellen-Dumoulin C, Munnich A, Viollet L (2004) Allelic heterogeneity of SMARD1 at the IGHMBP2 locus. Hum Mutat 23:525–526
14. Viollet L, Zarhrate M, Maystadt I, Estournet-Mathiaut B, Barois A, Desguerre I, Mayer M, Chabrol B, LeHeup B, Cusin V, Billette D V, Bonneau D, Saugier-Veber P, Touzery-De VA, Delaubier A, Kaplan J, Jeanpierre M, Feingold J, Munnich A (2004) Refined genetic mapping of autosomal recessive chronic distal spinal muscular atrophy to chromosome 11q13.3 and evidence of linkage disequilibrium in European families. Eur J Hum Genet 12:483–488
15. Guenther UP, Schuelke M, Bertini E, D'Amico A, Goemans N, Grohmann K, Hubner C, Varon R (2004) Genomic rearrangements at the IGHMBP2 gene locus in two patients with SMARD1. Hum Genet 115:319–326
16. Neitzel H (1986) A routine method for the establishment of permanent growing lymphoblastoid cell lines. Hum Genet 73:320–326
17. den Dunnen JT, Antonarakis SE (2000) Mutation nomenclature extensions and suggestions to describe complex mutations: a discussion. Hum Mutat 15:7–12
18. Pfaffl MW (2001) A new mathematical model for relative quantification in real-time RT-PCR. Nucleic Acids Res 29:e45
19. Vandesompele J, De PK, Pattyn F, Poppe B, Van RN, De PA, Speleman F (2002) Accurate normalization of real-time quantitative RT-PCR data by geometric averaging of multiple internal control genes. Genome Biol 3:research0034.1–research0034.11
20. Desai-Mehta A, Cerosaletti KM, Concannon P (2001) Distinct functional domains of nibrin mediate Mre11 binding, focus formation, and nuclear localization. Mol Cell Biol 21:2184–2191
21. Cox GA, Mahaffey CL, Frankel WN (1998) Identification of the mouse neuromuscular degeneration gene and mapping of a second site suppressor allele. Neuron 21:1327–1337
22. Sambrook J, Russel DW (2001) In vitro mutagenesis using double-stranded DNA templates: selection of mutants with DpnI. Molecular cloning. Cold Spring Harbor Laboratory Press, Cold Spring Harbor, New York
23. Schwannhäusser B, Gossen M, Dittmar G, Selbach M (2008) Global analysis of cellular protein translation by pulsed SILAC. Proteomics (in press)
24. Pitt M, Houlden H, Jacobs J, Mok Q, Harding B, Reilly M, Surtees R (2003) Severe infantile neuropathy with diaphragmatic weakness and its relationship to SMARD1. Brain 126:2682–2692
25. Collins JS, Schwartz CE (2002) Detecting polymorphisms and mutations in candidate genes. Am J Hum Genet 71:1251–1252
26. DePristo MA, Weinreich DM, Hartl DL (2005) Missense meanderings in sequence space: a biophysical view of protein evolution. Nat Rev Genet 6:678–687
27. Goldberg AL (2003) Protein degradation and protection against misfolded or damaged proteins. Nature 426:895–899
28. Obminska-Mrukowicz B, Szczypka M, Gaweda B (2006) Modulatory effects of chitosan adipate on the T and B lymphocyte subsets in mice. J Vet Sci 7:157–160
29. Hur DY, Lee MH, Kim JW, Kim JH, Shin YK, Rho JK, Kwack KB, Lee WJ, Han BG (2005) CD19 signalling improves the Epstein–Barr virus-induced immortalization of human B cell. Cell Prolif 38:35–45
30. Helmken C, Hofmann Y, Schoenen F, Oprea G, Raschke H, Rudnik-Schoneborn S, Zerres K, Wirth B (2003) Evidence for a modifying pathway in SMA discordant families: reduced SMN level decreases the amount of its interacting partners and Htra2-beta1. Hum Genet 114:11–21